A Three-Step Model for Protein–Gold Nanoparticle Adsorption

ARTICLE *in* THE JOURNAL OF PHYSICAL CHEMISTRY C · APRIL 2014

Impact Factor: 4.77 · DOI: 10.1021/jp411543y

THE JOURNAL OF PHYSICAL CHEMISTRY C

Article

pubs.acs.org/JPCC

A Three-Step Model for Protein–Gold Nanoparticle Adsorption

Ailin Wang, Karthikeshwar Vangala, Tam Vo, Dongmao Zhang, and Nicholas C. Fitzkee*

Department of Chemistry, Mississippi State University, Mississippi State, Mississippi 39762, United States

Supporting Information

ABSTRACT: Gold nanoparticles (AuNPs) are an attractive delivery vector in biomedicine because of their low toxicity and unique electronic and chemical properties. AuNP bioconjugates can be used in many applications, including nanomaterials, biosensing, and drug delivery. While the phenomenon of spontaneous protein–AuNP adsorption is well-known, the structural and mechanistic details of this interaction remain poorly understood. As a result, predicting the orientation and structure of proteins on the nanoparticle surface remains a challenge. New techniques are therefore needed to characterize the structural properties of proteins as they bind to AuNPs. We have developed a straightforward and rapid NMR-based approach to quantitatively characterize the protein–AuNP interaction. This approach is immune to the inner filter effect, which complicates fluorescence measurements, and it can be performed without prior centrifugation of samples. Using a data set of six proteins, ranging in size from 3 to 583 residues, we measured the stoichiometry of binding to AuNPs with a diameter of 15 nm. The stoichiometry of binding can be predicted based on simple geometric considerations assuming that proteins remain globular on the AuNP surface. Using our approach, we find that a protein lacking cysteine residues can be displaced from AuNPs using a small organothiol compound, but proteins with surface cysteines are resistant to displacement. From this data we develop a model for adsorption consisting of three steps: an initial reversible association step, a rearrangement/reorientation step on the AuNP surface, and a final cysteine-dependent "hardening" step, after which binding becomes irreversible.

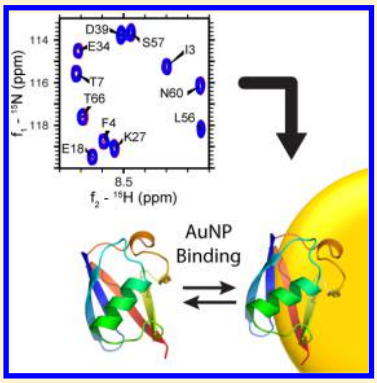

INTRODUCTION

Nanoparticles and nanoconjugates possess several unique properties that make them highly relevant in biomedical applications. Suitably designed nanoparticles are nontoxic, and their small size facilitates cellular uptake.[1] Nanoparticle systems have been engineered to include both a targeting mechanism and a therapeutic payload,[2−5] making nanoparticle-based disease treatment a reality. In contrast to polymer-based nanoparticles, gold nanoparticles (AuNPs) possess several unique optical and electronic properties that make them of particular interest. Specifically, both surface plasmon resonance (SPR) and surface-enhanced Raman spectroscopy (SERS) can be used to monitor changes on the AuNP surface,[6] and therefore AuNPs have unique biosensing applications as well.

It has been long recognized that protein molecules spontaneously adsorb to AuNPs.[7−9] This means that shortly after contact with any biological fluid, uncoated AuNPs will be completely coated with protein.[10−12] The initial formation of this protein corona is thought to occur rapidly, but over time the surface hardens as the exchange between adsorbed and free proteins slows down.[13,14] In AuNPs, this hardening process likely involves covalent bonding between cysteine thiols and AuNPs, but amines also may play a role.[15−17] Protein adsorption suggests an attractive approach to functionalizing AuNPs. Given the broad diversity of enzymatic functions, a protein-functionalized gold nanoconjugate would be very valuable to the biomedical community. Unfortunately, our understanding of the protein–AuNP interaction is limited, and a variety of behaviors have been observed. For example, recent experiments have demonstrated that the enzymes lysozyme and chymotrypsin experience a significant loss of activity when adsorbed to AuNPs,[18] and a similar result was seen for fibrinogen.[19] On the other hand, pepsin remains active when bound to AuNPs,[20] and adsorption enhances the stability of bovine catalase at high temperatures.[21] Additionally, while enzyme activity may diminish on the nanoparticle surface, proteins appear to retain their secondary structure as evidenced by circular dichroism (CD) measurements.[22] Thus, whether enzyme activity is retained upon adsorption appears to be a protein-specific effect. There is currently no way to predict whether proteins will retain their function when adsorbed to AuNPs.

While understanding the effects of AuNPs on protein structure is important, it is equally important to understand the overall stoichiometry and affinity of binding, as this reveals the extent of organization on the nanoparticle surface. Two methods currently are predominant: fluorescence spectroscopy and isothermal titration calorimetry (ITC). Fluorescence measurements monitor tryptophan quenching or enhancement as AuNPs are added to a protein solution.[23,24] Typical dissociation constants observed by fluorescence are in the 0.5−1.0 μM range.[25] However, a recent study found that the interpretation of fluorescence measurements can be severely complicated by the inner filtration effect because AuNPs can

Received: November 24, 2013
Revised: March 21, 2014
Published: March 21, 2014

absorb both excitation and fluorescence photons.[5] ITC has also been used to monitor adsorption, and calorimetric heats can be used to determine the energetics of binding. ITC is immune to the inner filter effect, and calorimetric stoichiometries and equilibrium constants are in general agreement with fluorescence measurements.[13,26] Nevertheless, a complete ITC titration can take several hours to complete, and thiol oxidation can contribute to the observed heats. Other quantitation methods have been proposed as well,[7,21] but these methods often require more elaborate sample preparation. The mechanism of binding is complicated by the fact that, for at least some systems, the kinetics of exchange are very slow, meaning that, at biologically relevant time scales, binding may not be at equilibrium.[14,27]

Biophysical NMR is a potential tool for examining both structure and stoichiometry on the AuNP surface. Amide proton chemical shifts are exquisitely sensitive to their environment, and a simple 2D HSQC spectrum can be used to monitor every backbone position in a protein.[28] Solution NMR has been successfully applied to study binding to gold clusters (2−5 nm in diameter),[29,30] and recent applications have probed surface heterogeneity by analyzing the spectral changes upon adsorption.[31] However, these studies have been limited to small systems; AuNPs larger than 10 nm tumble too slowly to be detected by conventional solution NMR.[29] An apparent exception is the recent report of ubiquitin (UBQ) adsorption on the surface of 12 nm AuNPs.[32] In this study, fast exchange between the bound and unbound form of UBQ was observed, allowing Calzolai et al. to investigate the protein interaction site through chemical shift perturbation. This data has been used to identify a potential mode of UBQ−AuNP interaction.[33]

Here, we present an extremely simple yet novel approach to quantifying protein adsorbed to AuNPs using NMR spectroscopy. The approach is nondisruptive and requires no centrifugation or chemical treatment to obtain accurate measurements, and following sample preparation, the total NMR instrument time is as little as 10 min. Using this approach on 15 nm AuNPs, we have measured adsorption capacity for five proteins, and we find that the adsorption capacity is well-predicted by geometric considerations. We have also employed a competition assay allowing us to measure protein binding and displacement directly. When combined with other work, our results suggest a model for binding where proteins initially associate and dissociate reversibly, with little deformation from their native, globular shape. Then, as covalent attachments form between the protein and AuNP, binding becomes irreversible, forming a hardened protein corona.

MATERIALS AND METHODS

GB3 Protein Preparation. The pET-11b plasmid containing the GB3 protein was a generous gift from Dr. Ad Bax (NIH). Protein expression and purification were based on the method of Ulmer et al.,[34] but additional steps were required to ensure the elimination of DNA from the final purified sample. This is because DNA is also capable of binding AuNPs,[35] and consistent results were not obtained until all DNA was removed from the sample (data not shown). Briefly, the plasmid was transformed by heat shock into competent Bl21(Star) DE3 cells (Invitrogen). A single colony was used to inoculate a 1 L culture in LB media (for 1D spectra and competition assays) or ^{15}N M9 media. Cells were incubated at 37 °C and induced with 1 mM isopropylthio-β-galactoside (IPTG) at an OD_{600} of 0.6. After induction, cells were allowed to express overnight at room temperature. Cells were harvested by centrifugation at 8000g for 20 min. After harvesting, the cells were resuspended in 50 mL of lysis buffer (50 mM NaCl, 20 mM NaH_2PO_4 pH 7.5, 5 mM EDTA, 0.5 mg/mL lysozyme). For K19C GB3, 50 mM DTT was added to ensure that all thiols were reduced. The resuspended cells were sonicated on ice in a Branson sonicator at power level 4 (2 min continuous pulse, 2 min rest). After lysis, the supernatant was incubated in an 85 °C water bath for 15 min, swirling every 3−4 min. The sample was cooled in an ice water bath, allowing most cellular proteins to precipitate. DNA was precipitated by adding 0.5% (w/v) streptomycin sulfate and gently stirring for 10 min. Insoluble proteins and DNA were removed by centrifuging at 18000g for 45 min. The supernatant was loaded on to a HiLoad 26/600 Superdex 75 pg gel filtration column equilibrated with 50 mM NaCl, 50 mM NaH_2PO_4, pH 7, 5 mM DTT. The collected fractions were further purified by anion exchange column (5 mL HiTrap Q FF). GB3 was eluted with a 1 M NaCl gradient over 50 mL. Pooled fractions were dialyzed in water overnight, frozen at −80 °C, and lyophilized for long-term storage. The K19C variant of GB3 was generated using the QuickChange II site-directed mutagenesis kit (Agilent). This mutation does not disrupt the protein structure.[36]

Pin1 WW Domain Preparation. A T7-inducible plasmid containing the His-tagged WW domain of human Pin1 (WW; residues 1−41) was purchased from GenScript (Piscataway, NJ). Protein expression was performed identically to GB3. Cells were resuspended in buffer A (150 mM NaCl, 20 mM HEPES pH 7.5, 20 mM imidazole) plus 0.5 mg/mL of lysozyme. After sonication, the lysate was clarified by centrifugation at 18000g for 45 min. The supernatant was loaded onto a 5 mL HisTrap FF column, and the Pin1 WW domain was eluted with buffer A + 800 mM imidazole gradient over 60 mL. After pooling fractions, thrombin was added to 1 U/mg of WW, and cleavage/dialysis was performed overnight into buffer A at 4 °C. 0.5 mL of benzamidine sepharose was equilibrated in buffer A and added to the dialyzed sample. After rocking on ice for 30 min the sample was centrifuged at 3800g for 10 min to remove the beads. The supernatant was loaded on to a HisTrap FF, and the flow through, containing purified Pin1, was further purified by gel filtration on a HiLoad 26/600 Superdex 75 pg column, equilibrated with buffer A.

Additional Protein Samples. Glutathione (GSH), bovine carbonic anhydrase (BCA), and bovine serum albumin (BSA) were purchased from Sigma-Aldrich and used without further purification. Fresh samples were prepared for each experiment by dissolving the lyophilized protein powder directly in to water. ^{15}N-labeled ubiquitin was expressed and purified using perchloric acid extraction as described previously.[37] The plasmid containing ubiquitin was a gift from Dr. David Fushman (University of Maryland). Concentrations for all samples were determined using the UV absorbance at 280 nm.[38]

Citrate-Stabilized AuNP Preparation. Gold(III) chloride trihydrate and sodium citrate dihydrate were purchased directly from Sigma-Aldrich. Gold nanoparticles were synthesized by the citric acid reduction method.[39] A 100 mL solution of 1 mM $HAuCl_4$ and a 10 mL solution of 38.8 mM Na-citrate were prepared using ultrapure water. The gold solution was heated to boiling, after which the Na-citrate solution was added. The mixture was kept boiling for 20 min. After centrifuging at 7700g for 40 min, the concentrated AuNPs (140 nM) were sonicated

dx.doi.org/10.1021/jp411543y | J. Phys. Chem. C 2014, 118, 8134−8142

for 6 min at power level 2 on a Branson sonicator. The size of 15 nm was confirmed based on TEM and UV−vis spectroscopy, where a maximum absorbance was observed at 520 nm (Supporting Information).[40,41]

Adsorption Capacity Measurements. 20 μM protein was prepared with 40 mM phosphate buffer at pH 7. After adding 6% D_2O and 270 μM trimethylsilylpropanoic acid (TMSP), protein samples were mixed with AuNPs at concentrations from 8 to 140 nM. Volumes were adjusted so that the total concentration of protein and the TMSP concentration were constant in all samples. The sample was incubated for approximately 1 h at room temperature to allow adequate time for the proteins to adsorb.[42] NMR spectra were recorded immediately afterward at a temperature of 25 °C. Proton 1D spectra were recorded on a 600 MHz Bruker Avance III cryoprobe-equipped NMR spectrometer using a jump-return experiment for water suppression.[43] The interpulse delay was set to 110 μs to select for proton resonances at 8.5 ppm, and an acquisition time of 80 ms was used. The total experiment time for each sample was 5 min.

NMR spectra were processed using TOPSPIN software. To measure the concentration of protein bound, the TMSP peak was used as a reference, and protein concentration was assessed by integrating the protein amide signal with and without AuNPs. In practice, the TOPSPIN "scale spectra" feature was used for integration, although this produced the same results as integrating the spectra directly. Using the known protein concentration without AuNPs (20 μM), it is possible to calculate how much protein is bound by the fraction of signal that was lost when AuNPs are added. If the total protein concentration is C_P, the total nanoparticle concentration is C_{NP}, and the ratio of integrated signals with and without AuNPs is r (where $r < 1$), then the number of proteins bound per nanoparticle (N) is

$$N = \frac{(1 - r)C_P}{C_{NP}} \quad (1)$$

Provided that binding kinetics are slow (~ms or longer), this equation can be used to determine the amount of bound protein, even if nanoparticles are not saturated. However, under saturating conditions, the maximum adsorption capacity can be determined. For typical values of C_P and C_{NP} used in our experiments (20 μM and 140 nM, respectively), the AuNPs will be >95% saturated if K_D is less than 0.5−1.0 μM. While typical K_D values are in the 4−350 nM range for protein−AuNP adsorption,[8] they can be as high as 1.0 μM.[25] Given this range of K_D values, we expect AuNPs to be very nearly saturated in our experiments. Furthermore, if binding were not saturated, it would be detectable in our experiments. While only two NMR samples are needed to calculate r (and thus N), in practice $(1 - r)C_P$ was plotted against C_{NP} and N was determined as the slope of the best-fit line from several samples. If binding were not saturated, one would expect to observe curvature in this plot. No such curvature was detected within the uncertainty of our experiments (Supporting Information). Thus, under these experimental conditions, binding is saturated, and N reflects the maximum adsorption capacity.

Under extreme conditions, where the protein concentration is comparable to the total concentration of binding sites on the AuNP, binding would not be saturated. While N would still be an accurate measurement of the number of proteins bound, N would underestimate the total adsorption capacity, leading to a systematic error in this value. A detailed treatment of this systematic error (Supporting Information) reveals that N is underestimated by at most 5% for the proteins used in this study. In practice, this is less than the experimental uncertainty of our measurements. When higher concentrations of AuNPs are used, binding is no longer saturated, and the data do not follow a linear trend. Under these conditions, the concentration of bound protein becomes difficult to quantify reliably because of the correspondingly low signal from unbound protein (data not shown).

Uncertainties for each protein concentration are reported as the sample standard deviation of at least three independently prepared samples. The adsorption capacity N was determined using weighted linear least-squares fitting of a plot of AuNP vs bound protein concentration. As described above, the slope of this line gives N.

Two-Dimensional NMR Experiments. 2D TROSY-HSQC spectra[44] were recorded using 20 μM ^{15}N-labeled GB3 in the presence of 40 nM AuNPs. This sample was compared to one prepared without AuNPs, and both samples were prepared identically to samples used for 1D experiments. An indirect acquisition time of 150 ms was used (300 complex points). Similar experiments were carried out using 30 μM UBQ in the presence of 50 nM AuNPs.

Table 1. Protein−AuNP Adsorption Capacities

	residues	R_G[a] (Å)	observed[b]	predicted[b]
GSH	3	3.75	1430 ± 90	1600
WW	45	10.52	165 ± 6	203
GB3	56	10.62	177 ± 20	199
UBQ	76	12.04	156 ± 12	155
BCA	259	17.17	63 ± 7	76
BSA	583	26.15	30 ± 10	33

[a]Calculated as described (Materials and Methods). [b]Reported as the number of molecules bound to a single 15 nm AuNP.

Protein Structure Calculations. The radius of gyration (R_G) for the proteins in Table 1 was calculated according to the formula

$$R_G = \sqrt{\frac{1}{N}\sum_{i=1}^{N}(\vec{x}_i - \vec{x})^2} \quad (2)$$

In this formula, $\vec{x}_i$ is the position of atom i in the structure, $\langle\vec{x}\rangle$ is the geometric center of the molecule, and N is the total number of (non-hydrogen) atoms. For crystal structures, all crystallographic waters and heteroatoms were first removed before calculating R_G. The PDB records used were 2OED (GB3),[34] 1I6C (WW),[45] 1UBQ (UBQ),[46] 1V9E (BCA),[47] and 3V03 (BSA).[48] For the Pin1 NMR structure, an average model was constructed from all models in the PDB file, and the best structure was chosen as the model with the lowest RMSD from the average. A value of 3.75 Å was reported previously as the aqueous R_G for GSH.[49]

MBI Competition Assays. 20 μM WT or K19C GB3 was mixed with 50 nM AuNP and incubated at room temperature for 2 days. 2-Mercaptobenzimidazole (MBI) was added to each sample to a final concentration of 100 μM, after which 1D proton NMR spectra were obtained. Protein adsorption was assessed using signals in the amide proton region from 8 to 9

dx.doi.org/10.1021/jp411543y | J. Phys. Chem. C 2014, 118, 8134−8142

ppm, whereas MBI concentration was measured using the strong aromatic signal at 7.1 ppm. A second measurement was carried out 24 h later.

RESULTS AND DISCUSSION

Consequences of AuNP Adsorption on Protein NMR Signals. Because of their large size relative to proteins, AuNPs will experience much slower rotational diffusion. When bound to AuNPs, proteins will adopt the rotational diffusion coefficient of the nanoparticles themselves. According to the Stokes–Einstein equation, the rotational diffusion time (τ_c) is related to the hydrodynamic radius of the protein–nanoparticle complex by

$$\tau_c = \frac{4\pi\eta {r_H}^3}{3k_B T} \quad (3)$$

In this equation, η is the solvent viscosity, r_H is the effective hydrodynamic radius of the protein, k_B is the Boltzmann constant, and T is the temperature.

For the 15 nm nanoparticles used in this study, the predicted τ_c is approximately 240 ns, and protein adsorption increases this time. The proton T_2 relaxation time for a system of this size is expected to be extremely short (less than 1 ms).[29] The protein is expected to experience a host of different chemical environments on the surface of the AuNP, and this will also contribute to line broadening in the bound state.[50] Therefore, NMR signals from nanoparticle-bound proteins are expected to be negligible. In the fast exchange regime (typically in the 10–100 μs time scale), the observed relaxation rate will be the population-weighted average of the free and bound forms, and line broadening will occur. In the slow exchange regime, observed here (see below), nanoparticle-bound protein will be invisible, and the unbound protein signal will not be broadened. In this sense, protein adsorption appears to be similar to protofibril formation in α-synuclein and Aβ peptides.[51,52] Given that the nanoparticle-bound "dark" state is invisible, if an appropriate reference is used, it is possible to quantify the binding to AuNPs based on the decrease in the integrated NMR signal (see eq 1).

GB3 Adsorption to AuNPs. GB3 is a compact, 56-residue protein with a well-resolved amide proton NMR spectrum. Initial titrations with GB3 and AuNPs were performed in the presence of trimethylsilylpropanoic acid (TMSP), a non-interacting reference compound. While some proteins are able to induce aggregation in AuNP samples, this was not observed for GB3 under our experimental conditions. No obvious change in the shape or position of the GB3 NMR spectrum is observed on addition of AuNPs, and the intensity decreases linearly with AuNP concentration (Figure 1A). This indicates that AuNP adsorption is within the slow exchange regime for GB3, and therefore a reduction in signal corresponds directly to AuNP binding. The linear behavior of bound protein vs AuNP concentration suggests that the nanoparticles are saturated (Figure 1B). Previous studies have measured K_D values in the range of 4 nM–1.0 μM,[8,25] and it is expected that AuNPs will be saturated for the conditions used in our experiments. Under saturating conditions, it is not straightforward to measure an equilibrium constant; however, the degree of binding can be determined by measuring the slope of the observed binding behavior. For GB3, the measured adsorption capacity is 177 ± 20 per nanoparticle.

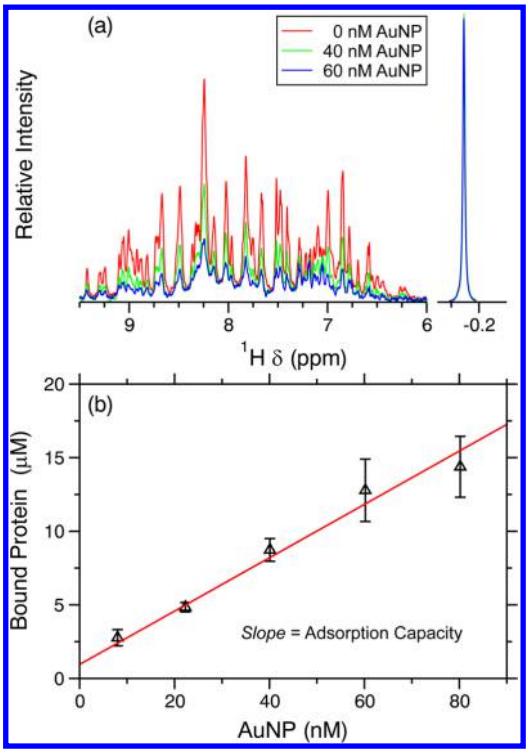

Figure 1. Behavior of GB3 in the presence of AuNPs. (a) Amide proton NMR region in GB3 with various concentrations of AuNPs. GB3 without AuNPs (red) is overlaid with spectra of 40 nM and 60 nM AuNPs. The internal reference peak for TMSP is shown at right. Peaks decay linearly, and line widths do not change significantly. (b) Concentration of bound GB3 is plotted vs various concentrations of AuNPs. The slope of the best-fit line (red) is the adsorption capacity of AuNP for GB3.

Two-dimensional NMR spectroscopy was also used to analyze adsorption. Specifically, a 2D ^{1}H–^{15}N TROSY-HSQC was measured under conditions where 40% of the protein was adsorbed (Figure 2). As expected from the 1D spectrum, no significant chemical shifts were observed for any of the residues (Supporting Information). Intensities and ^{15}N line widths were also measured for this sample, and no significant deviations from the average were identified. Peak intensities indicated that all residues had decreased by approximately 40% from their

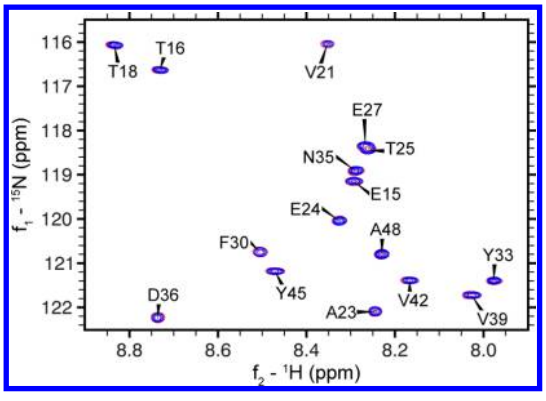

Figure 2. Excerpt from ^{15}N–^{1}H TROSY spectrum of GB3, with (blue) and without (red) AuNPs. Contours have been scaled to account for the intensity loss when AuNPs are present. Otherwise, the spectra are nearly superimposable. Similar behavior is observed for all other residues in GB3 (Supporting Information).

dx.doi.org/10.1021/jp411543y | J. Phys. Chem. C 2014, 118, 8134–8142

unbound values, and line widths were comparable between bound GB3 and GB3 in the absence of AuNPs (Supporting Information). In light of previous experiments with human ubiquitin, where substantial shifts were observed in the bound state,[32] this result was surprising, and it led us to investigate the behavior of several additional small proteins.

Creating a Data Set of Adsorption Behavior. To test the generality of our observations with GB3, the adsorption capacity of five additional protein samples was measured. These proteins include glutathione (GSH), the WW domain of human Pin1 (WW), ubiquitin (UBQ), bovine carbonic anhydrase 2 (BCA), and bovine serum albumin (BSA). For all of the proteins, we observed similar slow-exchange behavior as we did for GB3. For all proteins, the adsorption capacity was determined from the slope of a plot of bound protein vs AuNP concentration (Table 1).

The spectrum of BSA did not change substantially when AuNPs were added, but interpreting BSA binding was complicated by two factors: First, unlabeled BSA was used in our experiments, and fast T_2 relaxation for a protein of this size (66 kDa) results in broad peaks, even for unbound BSA. Second, the BSA 1D proton spectra were highly sensitive to pH (data not shown). This behavior likely results from structural changes in BSA in solution, and pH-dependent effects have been documented before in this protein.[53,54] These changes appeared even in buffered solution, and this complicated the measurement of the BSA adsorption capacity. Our measured value, 30 ± 10 BSA molecules per AuNP, is reported as the average of five independent measurements taken at an AuNP concentration of 140 nM AuNP. A previous study measured a surface coverage of $(3.7 \pm 0.2) \times 10^{12}$ molecules cm^{-2} for BSA on AuNPs.[25] For a 15 nm AuNP, this corresponds to 26 ± 1 molecules per AuNP, in good agreement with our measurement.

After adding the AuNPs into the bovine carbonic anhydrase sample, the dark red nanoparticles turned purple in color, indicating that AuNP aggregation had occurred. This aggregation occurred over several hours, much slower than the time scale of initial adsorption and AuNP surface coverage. Because NMR monitors the unbound protein only, this aggregation does not affect our adsorption capacity measurements. Indeed, irreversibly adsorbed protein in an aggregated state cannot contribute to the solution NMR signal, and aggregated samples are expected to be more reliable than nonaggregating samples provided that surface coverage is complete. Essentially, this exploits the same principle as sedimentation-based methods for quantifying AuNP binding, without the requirement for high-speed centrifugation. This is an advantage of our method because aggregated samples can be measured *in situ* without taking additional time for centrifugation.

To test whether our approach can be used on smaller molecules in addition to proteins, we measured the binding of 2-mercaptobenzimidazole (MBI) to AuNPs (Supporting Information). MBI is an organothiol ligand which can bind to AuNP by forming a stable Au−S bond.[55] The adsorption capacity of MBI measured here (1490 MBI per AuNP, or 350 pmol cm^{-2}) is smaller than previously determined values (570 pmol cm^{-2}).[56] While these values are in the same approximate range, the difference is statistically significant. Work is ongoing to determine the source of this discrepancy.

For all of the proteins, a linear fit was used to measure the adsorption capacity. Including shimming and sample changes, the total time for each protein was approximately 30 min on a 600 MHz cryoprobe-equipped NMR spectrometer (5 min each for a reference and four different AuNP concentrations). However, if binding is known to be saturated, a two-point measurement is sufficient, requiring only about 10 min of total NMR time to record the stoichiometry. Additionally, the approach is amenable to lower fields and less sensitive probes, and we have obtained similar results using a 300 MHz NMR with a conventional probe (data not shown).

Ubiquitin Adsorption Kinetics. A previous study by Calzolai et al. observed fast exchange (~10−100 μs) between the adsorbed and free protein states of UBQ. In this study, certain chemical shifts were perturbed as the AuNP concentration was gradually increased.[32] Unfortunately, we have not been able to reproduce these observations, despite working at similar experimental conditions and with similarly sized AuNPs (12 nm vs 15 nm in diameter). Indeed, UBQ appears to behave similarly to other proteins in our data set, and we detect no significant chemical shift changes or line broadening for UBQ in the presence of AuNPs (Figure 3,

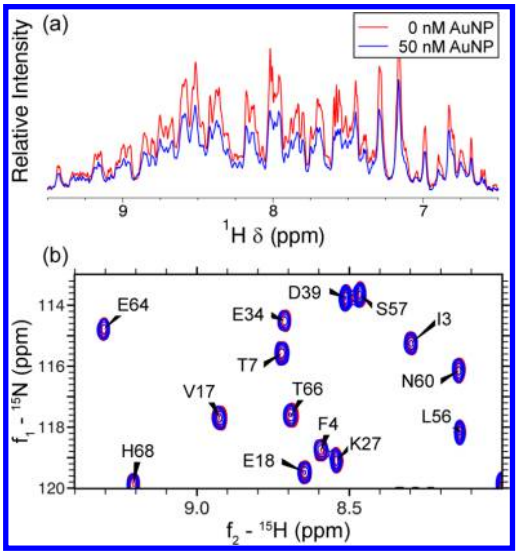

Figure 3. NMR spectra of UBQ in the presence (blue) and absence (red) of AuNPs. (a) A 1D proton spectrum comparing UBQ samples with and without 50 nMAuNPs. As with other proteins, there are no peak shifts, and line broadening is minimal. (b) Excerpt from ^{15}N−^{1}H TROSY spectrum of UBQ, showing no difference in peak positions when 50 nM AuNPs are added to 30 μM UBQ. The contours have been scaled so that intensities are comparable; actual intensities are shown in (a). This behavior is observed for all residues (Supporting Information).

Supporting Information). One possible explanation for this discrepancy is differences in sample preparation. Calzolai et al. obtained ^{15}N-labeled UBQ commercially, while we purified the protein directly from a bacterial expression system.[37] The commercial preparation may contain contaminants, such as DNA, that would affect adsorption.[35] As assessed by the UV absorbance at 260 vs 280 nm, our sample does not appear to contain DNA contaminants. Given the fast T_2 relaxation expected for proteins on the AuNP surface, a chemical shift perturbation from fast exchange should be associated with a corresponding increase in line width;[57] nevertheless, the possibility of identifying specific sites capable of interacting

dx.doi.org/10.1021/jp411543y | J. Phys. Chem. C 2014, 118, 8134−8142

with AuNPs is highly intriguing, and work is ongoing to identify the source of this discrepancy.

Are Proteins Compact on AuNPs? Using simple geometric considerations, it is possible to predict the adsorption capacity of a spherical AuNP. This approach has been applied to quantum dots and polymer-based nanoparticles.[58,59] We have adopted a similar approach, using the radius of gyration (R_G) calculated from the protein structure. While the R_G does not directly capture the longest dimension of the protein, and it cannot account for nonspherical shapes, it roughly represents the occluded surface on the AuNP itself. Using this metric, the predicted maximum adsorption capacity (N_{max}) is given by

$$N_{max} = \frac{4{R_{AuNP}}^2}{{R_G}^2} \quad (4)$$

For AuNPs of 15 nm diameter, the agreement between the predicted and measured adsorption capacity is very good (Figure 4 and Table 1). No parameters are adjusted to create the curve in Figure 4, yet the Pearson correlation coefficient is 0.9998 ($p < 7.5 \times 10^{-11}$).

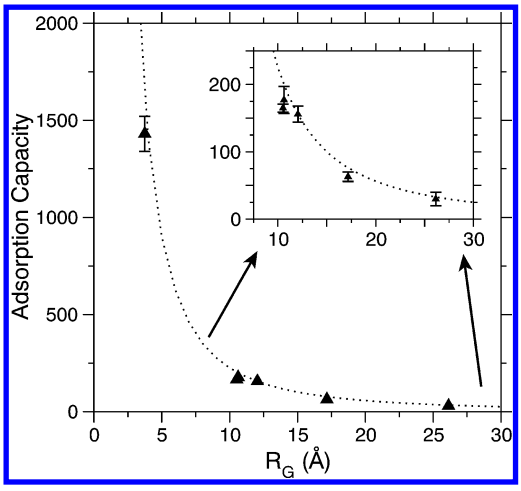

Figure 4. Adsorption capacity of AuNPs for differently sized proteins. The dotted line represents the predicted maximum adsorption capacity assuming a folded protein R_G. Triangles indicate experimental measurements. The same data are plotted in the inset to illustrate error bars, which are too small to visualize when GSH is included.

MBI Competition. Previously, we used MBI as a probe to examine the stability of protein–AuNP complexes.[42] Wild-type (WT) GB3 does not have any cysteine residues, and SERS experiments suggested that it could be displaced by the addition of MBI. By monitoring the NMR signals of GB3 and MBI, we are able to examine this displacement directly (Figure 5). AuNP and GB3 were mixed and allowed to incubate at room temperature for 2 days. Then, MBI was added to test whether GB3 could be removed from AuNPs. To test the importance of surface Cys residues, we used both WT and K19C GB3. Initially, both WT and K19C GB3 were observed to bind to AuNPs similarly (Figure 5a), but after addition of MBI, the concentration of unbound GB3 is observed to increase, indicating that WT GB3 can be displaced by MBI. This reaction occurs within 15 min after adding MBI, and it does not change significantly after 24 h. K19C GB3 behaves differently; MBI cannot displace this variant from the AuNP (Figure 5a, gray bars), and even after 24 h most of the protein remains bound to the AuNP surface.

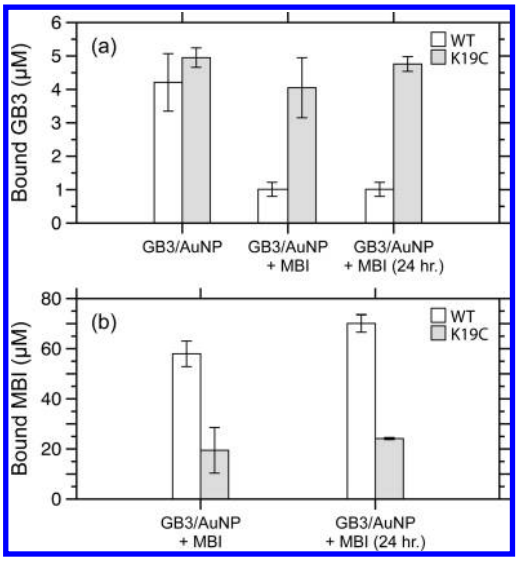

Figure 5. Competition of MBI with wild-type (WT) and K19C GB3. The concentration of GB3 (a) and MBI (b) bound to AuNPs was monitored after mixing GB3 with AuNPs and then adding MBI. Samples were prepared containing WT (no cysteines) and K19C GB3. Error bars represent the standard deviation from three independently prepared samples. MBI can effectively displace WT GB3, but the Cys residue in K19C prevents displacement. After 24 h, samples are essentially unchanged relative to initial preparation, suggesting that competition is relatively fast.

The same effect can be observed by examining the MBI signal (Figure 5b). MBI can bind in the WT GB3 sample (white bars), but it cannot bind in the K19C sample (gray bars). Ostensibly, this is because K19C cannot be displaced from AuNPs. Therefore, in the absence of surface cysteine residues, the protein can associate and dissociate reversibly from the AuNP. However, a single surface cysteine is enough to make protein association effectively irreversible over time.

A Model for Protein–AuNP Adsorption. Together, our data support a three-step model for protein–AuNP adsorption. In the first step, proteins experience reversible association to the AuNP surface (Figure 6). Given that no chemical shift perturbations are observed in our experiments, the average lifetime on the AuNP surface is on the order of 10–100 ms (or longer) so that exchange is slow on the NMR time scale. Once on the surface, the protein remains fairly globular, if not native. It is likely that the structure of some proteins is perturbed more than others, as this would account for the different enzymatic activities observed.[18,19,21] However, the overall shape is likely maintained; otherwise, the folded structure would not reliably predict the adsorption capacity. Similarly, the proteins are likely able to reorient on the AuNP to a small degree. This reorientation would ensure that a near-maximal number of proteins are able to bind. Finally, over time most proteins will become irreversibly attached to the AuNP. This hardening process will occur in proteins containing surface cysteine residues, since these residues can irreversibly oxidize on the AuNP surface, as demonstrated by the K19C GB3–MBI competition experiments. Our experiments with WT GB3 indicate that proteins can be displaced by organothiols, and they appear to resist irreversible hardening. Hardening could occur if it is mediated by amines or other moieties, and this is

dx.doi.org/10.1021/jp411543y | J. Phys. Chem. C 2014, 118, 8134–8142

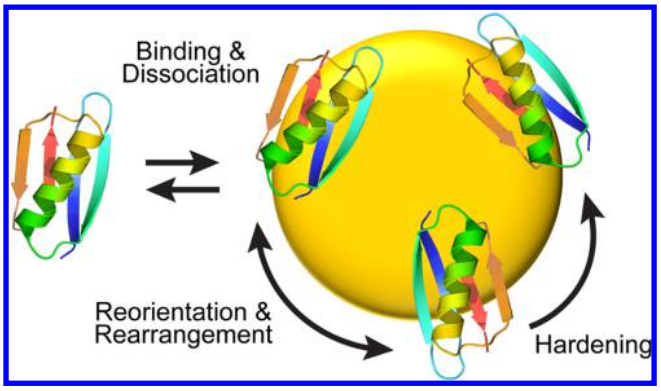

Figure 6. Three-step model for protein adsorption on 15 nm AuNPs. In the initial binding stage, the protein reversibly associates with the AuNP surface. The protein is then able to reposition itself to maximize the available AuNP surface for binding. Proteins are likely not natively folded on the surface but remain compact and globular. After a time, the coating becomes irreversibly bound. This "hardening" is greatly facilitated by surface Cys residues. Nanoparticles and GB3 are not drawn to scale.

likely the cause for hardening in other classes of nanoparticles.[14,27] However, irreversible attachment does not appear to occur in the time scale of our experiments. For proteins lacking cysteine, only the reversible binding step is observed.

Once protein adsorption occurs, it is effectively invisible to NMR. We observe no change in the NMR spectra up to 3 days after adsorption (data not shown), but our method is only able to detect stoichiometry and not structural rearrangement. Therefore, it is possible the protein−protein interactions can lead to additional effects that are undetectable by this method. Similarly, we cannot rule out that additional surface restructuring occurs as part of the hardening process that we cannot detect. Indeed, our own SPR and SERS measurements indicate that restructuring occurs for several days after initial adsorption,[42] and additional protein interactions may take place once the initial corona is formed.[14] Finally, we emphasize that our study focused on 15 nm AuNPs; the effects may be quite different on larger AuNPs where the surface exhibits less curvature.[18] The complications may also be protein-specific,[60] and continued study is needed to understand the mechanism of AuNP adsorption.

CONCLUSIONS

We have presented an NMR-based approach for characterizing the stoichiometry of molecular binding to AuNPs. The approach is straightforward and rapid, and under saturating conditions, it is possible to estimate the maximum adsorption capacity. We measured the stoichiometry for a data set of six proteins, and we found that the adsorption capacity can be predicted using the radius of gyration calculated from the folded protein structure. Our data support a simple model for protein adsorption on 15 nm AuNPs: Initially, protein binding is reversible, and the structural changes upon adsorption are minor, allowing the protein to remain globular. Once on the surface, the protein is able to reorient, making room for neighboring proteins so that the adsorption capacity is maximized. Finally, cysteine-containing proteins experience a hardening step where binding becomes irreversible. This final step is likely associated with surface restructuring that would lead to changes in the SPR and SERS signal from the bound protein. The methodology outlined here can be easily applied to other bioconjugate systems with tight binding, and future work will investigate the behavior of proteins on other nanoparticle systems.

ASSOCIATED CONTENT

Supporting Information

Complete spectral data for GB3 and UBQ, along with adsorption curves for all other compounds; a detailed error analysis of the method assuming equilibrium binding. This material is available free of charge via the Internet at http://pubs.acs.org.

AUTHOR INFORMATION

Corresponding Author

*E-mail: nfitzkee@chemistry.msstate.edu (N.C.F.).

Notes

The authors declare no competing financial interest.

ACKNOWLEDGMENTS

The authors thank Dr. Ad Bax for supplying the plasmid for GB3 expression and Dr. David Fushman for supplying the ubiquitin plasmid. This work was funded by the Henry Family Foundation, an NSF CAREER Award (CHE 1151057), an NSF fund (EPS 0903787), and a seed grant provided to D.Z. from Agricultural Research Service, U.S. Department of Agriculture, under Project Number No. 5864022729.

ABBREVIATIONS

BCA, bovine carbonic anhydrase; BSA, bovine serum albumin; GSH, glutathione; MBI, 2-mercaptobenzimidazole; TMSP, trimethylsilylpropanoic acid; UBQ, ubiquitin; WW, Pin1 WW domain.

REFERENCES

(1) Giljohann, D. A.; Seferos, D. S.; Daniel, W. L.; Massich, M. D.; Patel, P. C.; Mirkin, C. A. Gold Nanoparticles for Biology and Medicine. *Angew. Chem., Int. Ed.* **2010**, *49* (19), 3280−3294.

(2) Ghosh, P.; Han, G.; De, M.; Kim, C. K.; Rotello, V. M. Gold Nanoparticles in Delivery Applications. *Adv. Drug Delivery Rev.* **2008**, *60* (11), 1307−1315.

(3) Davis, M. E.; Chen, Z.; Shin, D. M. Nanoparticle Therapeutics: an Emerging Treatment Modality for Cancer. *Nat. Rev. Drug Discovery* **2008**, *7* (9), 771−782.

(4) Zheng, D.; Giljohann, D. A.; Chen, D. L.; Massich, M. D.; Wang, X. Q.; Iordanov, H.; Mirkin, C. A.; Paller, A. S. Topical Delivery of siRNA-Based Spherical Nucleic Acid Nanoparticle Conjugates for Gene Regulation. *Proc. Natl. Acad. Sci. U. S. A.* **2012**, *109* (30), 11975−11980.

(5) Ameer, F. S.; Ansar, S. M.; Hu, W.; Zou, S.; Zhang, D. Inner Filter Effect on Surface Enhanced Raman Spectroscopic Measurement. *Anal. Chem.* **2012**, *84* (20), 8437−8441.

(6) Blakey, I.; Merican, Z.; Thurecht, K. J. A Method for Controlling the Aggregation of Gold Nanoparticles: Tuning of Optical and Spectroscopic Properties. *Langmuir* **2013**, *29* (26), 8266−8274.

(7) Geoghegan, W. D.; Ackerman, G. A. Adsorption of Horseradish Peroxidase, Ovomucoid and Anti-Immunoglobulin to Colloidal Gold for the Indirect Detection of Concanavalin A, Wheat Germ Agglutinin and Goat Anti-Human Immunoglobulin G on Cell Surfaces at the Electron Microscopic Level: a New Method, Theory and Application. *J. Histochem. Cytochem.* **1977**, *25* (11), 1187−1200.

(8) De Roe, C.; Courtoy, P. J.; Baudhuin, P. A Model of Protein-Colloidal Gold Interactions. *J. Histochem. Cytochem.* **1987**, *35* (11), 1191−1198.

(9) Zhang, D.; Neumann, O.; Wang, H.; Yuwono, V. M.; Barhoumi, A.; Perham, M.; Hartgerink, J. D.; Wittung-Stafshede, P.; Halas, N. J.

Gold Nanoparticles Can Induce the Formation of Protein-based Aggregates at Physiological pH. *Nano Lett.* **2009**, *9* (2), 666−671.
(10) Lynch, I.; Salvati, A.; Dawson, K. A. Protein-Nanoparticle Interactions: What Does the Cell See? *Nat. Nanotechnol.* **2009**, *4* (9), 546−547.
(11) Walczyk, D.; Bombelli, F. B.; Monopoli, M. P.; Lynch, I.; Dawson, K. A. What the Cell "Sees" in Bionanoscience. *J. Am. Chem. Soc.* **2010**, *132* (16), 5761−5768.
(12) Wang, F.; Yu, L.; Monopoli, M. P.; Sandin, P.; Mahon, E.; Salvati, A.; Dawson, K. A. The Biomolecular Corona is Retained During Nanoparticle Uptake and Protects the Cells from the Damage Induced by Cationic Nanoparticles until Degraded in the Lysosomes. *Nanomedicine: Nanotechnol., Biol. Med.* **2013**, *9* (8), 1159−1168.
(13) Goy-López, S.; Juárez, J.; Alatorre-Meda, M.; Casals, E.; Puntes, V. F.; Taboada, P.; Mosquera, V. Physicochemical Characteristics of Protein−NP Bioconjugates: The Role of Particle Curvature and Solution Conditions on Human Serum Albumin Conformation and Fibrillogenesis Inhibition. *Langmuir* **2012**, *28* (24), 9113−9126.
(14) Milani, S.; Baldelli Bombelli, F.; Pitek, A. S.; Dawson, K. A.; Rädler, J. Reversible versus Irreversible Binding of Transferrin to Polystyrene Nanoparticles: Soft and Hard Corona. *ACS Nano* **2012**, *6* (3), 2532−2541.
(15) Leff, D. V.; Brandt, L.; Heath, J. R. Synthesis and Characterization of Hydrophobic, Organically-Soluble Gold Nanocrystals Functionalized with Primary Amines. *Langmuir* **1996**, *12* (20), 4723−4730.
(16) Gomez, S.; Philippot, K.; Colliere, V.; Chaudret, B.; Senocq, F.; Lecante, P. Gold Nanoparticles from Self-Assembled Gold() Amine Precursors. *Chem. Commun. (Cambridge, U. K.))* **2000**, *0* (19), 1945−1946.
(17) Selvakannan, P. R.; Mandal, S.; Phadtare, S.; Pasricha, R.; Sastry, M. Capping of Gold Nanoparticles by the Amino Acid Lysine Renders Them Water-Dispersible. *Langmuir* **2003**, *19* (8), 3545−3549.
(18) Gagner, J. E.; Lopez, M. D.; Dordick, J. S.; Siegel, R. W. Effect of Gold Nanoparticle Morphology on Adsorbed Protein Structure and Function. *Biomaterials* **2011**, *32* (29), 7241−7252.
(19) Deng, Z. J.; Liang, M.; Monteiro, M.; Toth, I.; Minchin, R. F. Nanoparticle-Induced Unfolding of Fibrinogen Promotes Mac-1 Receptor Activation and Inflammation. *Nat. Nanotechnol.* **2011**, *6* (1), 39−44.
(20) Gole, A.; Dash, C.; Ramakrishnan, V.; Sainkar, S. R.; Mandale, A. B.; Rao, M.; Sastry, M. Pepsin−Gold Colloid Conjugates: Preparation, Characterization, and Enzymatic Activity. *Langmuir* **2001**, *17* (5), 1674−1679.
(21) Bailes, J.; Gazi, S.; Ivanova, R.; Soloviev, M. Effect of Gold Nanoparticle Conjugation on the Activity and Stability of Functional Proteins. In *Nanoparticles in Biology and Medicine*, Soloviev, M., Ed.; Humana Press: New York, 2012; Vol. *906*, pp 89−99.
(22) Lacerda, S. H. D. P.; Park, J. J.; Meuse, C.; Pristinski, D.; Becker, M. L.; Karim, A.; Douglas, J. F. Interaction of Gold Nanoparticles with Common Human Blood Proteins. *ACS Nano* **2009**, *4* (1), 365−379.
(23) Wangoo, N.; Suri, C. R.; Shekhawat, G. Interaction of Gold Nanoparticles with Protein: A Spectroscopic Study to Monitor Protein Conformational Changes. *Appl. Phys. Lett.* **2008**, *92* (13), 133104−133103.
(24) Sen, T.; Mandal, S.; Haldar, S.; Chattopadhyay, K.; Patra, A. Interaction of Gold Nanoparticle with Human Serum Albumin (HSA) Protein Using Surface Energy Transfer. *J. Phys. Chem. C* **2011**, *115* (49), 24037−24044.
(25) Brewer, S. H.; Glomm, W. R.; Johnson, M. C.; Knag, M. K.; Franzen, S. Probing BSA Binding to Citrate-Coated Gold Nanoparticles and Surfaces. *Langmuir* **2005**, *21* (20), 9303−9307.
(26) Cedervall, T.; Lynch, I.; Lindman, S.; Berggard, T.; Thulin, E.; Nilsson, H.; Dawson, K. A.; Linse, S. Understanding the Nanoparticle-Protein Corona using Methods to Quantify Exchange Rates and Affinities of Proteins for Nanoparticles. *Proc. Natl. Acad. Sci. U. S. A.* **2007**, *104* (7), 2050−2055.
(27) Monopoli, M. P.; Aberg, C.; Salvati, A.; Dawson, K. A. Biomolecular Coronas Provide the Biological Identity of Nanosized Materials. *Nat. Nanotechnol.* **2012**, *7* (12), 779−786.
(28) Medek, A.; Hajduk, P. J.; Mack, J.; Fesik, S. W. The Use of Differential Chemical Shifts for Determining the Binding Site Location and Orientation of Protein-Bound Ligands. *J. Am. Chem. Soc.* **2000**, *122* (6), 1241−1242.
(29) Hostetler, M. J.; Wingate, J. E.; Zhong, C.-J.; Harris, J. E.; Vachet, R. W.; Clark, M. R.; Londono, J. D.; Green, S. J.; Stokes, J. J.; Wignall, G. D.; et al. Alkanethiolate Gold Cluster Molecules with Core Diameters from 1.5 to 5.2 nm: Core and Monolayer Properties as a Function of Core Size. *Langmuir* **1998**, *14* (1), 17−30.
(30) Song, Y.; Harper, A. S.; Murray, R. W. Ligand Heterogeneity on Monolayer-Protected Gold Clusters. *Langmuir* **2005**, *21* (12), 5492−5500.
(31) Liu, X.; Yu, M.; Kim, H.; Mameli, M.; Stellacci, F. Determination of Monolayer-Protected Gold Nanoparticle Ligand−Shell Morphology Using NMR. *Nat. Commun.* **2012**, *3*, 1182.
(32) Calzolai, L.; Franchini, F.; Gilliland, D.; Rossi, F. Protein−Nanoparticle Interaction: Identification of the Ubiquitin−Gold Nanoparticle Interaction Site. *Nano Lett.* **2010**, *10* (8), 3101−3105.
(33) Brancolini, G.; Kokh, D. B.; Calzolai, L.; Wade, R. C.; Corni, S. Docking of Ubiquitin to Gold Nanoparticles. *ACS Nano* **2012**, *6* (11), 9863−9878.
(34) Ulmer, T. S.; Ramirez, B. E.; Delaglio, F.; Bax, A. Evaluation of Backbone Proton Positions and Dynamics in a Small Protein by Liquid Crystal NMR Spectroscopy. *J. Am. Chem. Soc.* **2003**, *125* (30), 9179−9191.
(35) Hurst, S. J.; Lytton-Jean, A. K. R.; Mirkin, C. A. Maximizing DNA Loading on a Range of Gold Nanoparticle Sizes. *Anal. Chem.* **2006**, *78* (24), 8313−8318.
(36) Siriwardana, K.; Wang, A.; Vangala, K.; Fitzkee, N.; Zhang, D. Probing the Effects of Cysteine Residues on Protein Adsorption onto Gold Nanoparticles Using Wild-Type and Mutated GB3 Proteins. *Langmuir* **2013**, *29* (35), 10990−10996.
(37) Burschowsky, D.; Rudolf, F.; Rabut, G.; Herrmann, T.; Matthias, P.; Wider, G. Structural Analysis of the Conserved Ubiquitin-binding Motifs (UBMs) of the Translesion Polymerase iota in Complex with Ubiquitin. *J. Biol. Chem.* **2011**, *286* (2), 1364−1373.
(38) Grimsley, G. R.; Pace, C. N. Spectrophotometric Determination of Protein Concentration. In *Current Protocols in Protein Science*; John Wiley & Sons, Inc.: New York, 2001.
(39) Freeman, R. G.; Hommer, M. B.; Grabar, K. C.; Jackson, M. A.; Natan, M. J. Ag-Clad Au Nanoparticles: Novel Aggregation, Optical, and Surface-Enhanced Raman Scattering Properties. *J. Phys. Chem.* **1996**, *100* (2), 718−724.
(40) Link, S.; El-Sayed, M. A. Size and Temperature Dependence of the Plasmon Absorption of Colloidal Gold Nanoparticles. *J. Phys. Chem. B* **1999**, *103* (21), 4212−4217.
(41) Jain, P. K.; Lee, K. S.; El-Sayed, I. H.; El-Sayed, M. A. Calculated Absorption and Scattering Properties of Gold Nanoparticles of Different Size, Shape, and Composition: Applications in Biological Imaging and Biomedicine. *J. Phys. Chem. B* **2006**, *110* (14), 7238−7248.
(42) Vangala, K.; Ameer, F.; Salomon, G.; Le, V.; Lewis, E.; Yu, L.; Liu, D.; Zhang, D. Studying Protein and Gold Nanoparticle Interaction Using Organothiols as Molecular Probes. *J. Phys. Chem. C* **2012**, *116* (5), 3645−3652.
(43) Plateau, P.; Gueron, M. Exchangeable Proton NMR without Base-Line Distorsion, using New Strong-Pulse Sequences. *J. Am. Chem. Soc.* **1982**, *104* (25), 7310−7311.
(44) Pervushin, K.; Riek, R.; Wider, G.; Wüthrich, K. Attenuated T2 Relaxation by Mutual Cancellation of Dipole−Dipole Coupling and Chemical Shift Anisotropy Indicates an Avenue to NMR Structures of Very Large Biological Macromolecules in Solution. *Proc. Natl. Acad. Sci. U. S. A.* **1997**, *94* (23), 12366−12371.
(45) Wintjens, R.; Wieruszeski, J. M.; Drobecq, H.; Rousselot-Pailley, P.; Buee, L.; Lippens, G.; Landrieu, I. ^{1}H NMR Study on the Binding

of Pin1 Trp-Trp Domain with Phosphothreonine Peptides. *J. Biol. Chem.* **2001**, *276* (27), 25150−25156.
(46) Vijay-Kumar, S.; Bugg, C. E.; Cook, W. J. Structure of Ubiquitin Refined at 1.8 A Resolution. *J. Mol. Biol.* **1987**, *194* (3), 531−544.
(47) Saito, R.; Sato, T.; Ikai, A.; Tanaka, N. Structure of Bovine Carbonic Anhydrase II at 1.95 Å Resolution. *Acta Crystallogr., Sect. D: Biol. Crystallogr.* **2004**, *60* (Pt 4), 792−795.
(48) Majorek, K. A.; Porebski, P. J.; Dayal, A.; Zimmerman, M. D.; Jablonska, K.; Stewart, A. J.; Chruszcz, M.; Minor, W. Structural and Immunologic Characterization of Bovine, Horse, and Rabbit Serum Albumins. *Mol. Immunol.* **2012**, *52* (3−4), 174−182.
(49) Zhang, R.; Wu, W.; Luo, S. Different Behaviors of Glutathione in Aqueous and DMSO Solutions: Molecular Dynamics Simulation and NMR Experimental Study. *J. Solution Chem.* **2011**, *40* (10), 1784−1795.
(50) Badia, A.; Gao, W.; Singh, S.; Demers, L.; Cuccia, L.; Reven, L. Structure and Chain Dynamics of Alkanethiol-Capped Gold Colloids. *Langmuir* **1996**, *12* (5), 1262−1269.
(51) Bodner, C. R.; Dobson, C. M.; Bax, A. Multiple Tight Phospholipid-Binding Modes of Alpha-Synuclein Revealed by Solution NMR Spectroscopy. *J. Mol. Biol.* **2009**, *390* (4), 775−790.
(52) Fawzi, N. L.; Ying, J.; Torchia, D. A.; Clore, G. M. Kinetics of Amyloid Beta Monomer-to-Oligomer Exchange by NMR Relaxation. *J. Am. Chem. Soc.* **2010**, *132* (29), 9948−9951.
(53) Carter, D. C.; Ho, J. X. Structure of Serum Albumin. *Adv. Protein Chem.* **1994**, *45*, 153−203.
(54) Khan, M. Y. Direct Evidence for the Involvement of Domain III in the N-F Transition of Bovine Serum Albumin. *Biochem. J.* **1986**, *236* (1), 307−310.
(55) Doneux, T.; Tielens, F.; Geerlings, P.; Buess-Herman, C. Experimental and Density Functional Theory Study of the Vibrational Properties of 2-Mercaptobenzimidazole in Interaction with Gold. *J. Phys. Chem. A* **2006**, *110* (39), 11346−11352.
(56) Zhang, D.; Ansar, S. M. Ratiometric Surface Enhanced Raman Quantification of Ligand Adsorption onto a Gold Nanoparticle. *Anal. Chem.* **2010**, *82* (13), 5910−5914.
(57) Palmer, A. G. NMR Characterization of the Dynamics of Biomacromolecules. *Chem. Rev.* **2004**, *104* (8), 3623−3640.
(58) Mattoussi, H.; Mauro, J. M.; Goldman, E. R.; Anderson, G. P.; Sundar, V. C.; Mikulec, F. V.; Bawendi, M. G. Self-Assembly of CdSe−ZnS Quantum Dot Bioconjugates Using an Engineered Recombinant Protein. *J. Am. Chem. Soc.* **2000**, *122* (49), 12142−12150.
(59) Lindman, S.; Lynch, I.; Thulin, E.; Nilsson, H.; Dawson, K. A.; Linse, S. Systematic Investigation of the Thermodynamics of HSA Adsorption to N-iso-propylacrylamide/N-tert-butylacrylamide Copolymer Nanoparticles. Effects of Particle Size and Hydrophobicity. *Nano Lett.* **2007**, *7* (4), 914−920.
(60) Tellechea, E.; Wilson, K. J.; Bravo, E.; Hamad-Schifferli, K. Engineering the Interface between Glucose Oxidase and Nanoparticles. *Langmuir* **2012**, *28* (11), 5190−5200.